



# Distinguishing the Origin of Eccentric Black Hole Mergers with Gravitational-wave Spin Measurements

Jakob Stegmann<sup>1</sup> , Davide Gerosa<sup>2,3</sup> , Isobel Romero-Shaw<sup>4,5,6</sup> , Giulia Fumagalli<sup>2,3</sup> , Hiromichi Tagawa<sup>7</sup> , and Lorenz Zwick<sup>8</sup>

<sup>1</sup>Max Planck Institute for Astrophysics, Karl-Schwarzschild-Str. 1, 85748 Garching, Germany; [jstegmann@mpa-garching.mpg.de](mailto:jstegmann@mpa-garching.mpg.de)

<sup>2</sup>Dipartimento di Fisica “G. Occhialini,” Università degli Studi di Milano-Bicocca, Piazza della Scienza 3, 20126 Milano, Italy

<sup>3</sup>INFN, Sezione di Milano-Bicocca, Piazza della Scienza 3, 20126 Milano, Italy

<sup>4</sup>Department of Applied Mathematics and Theoretical Physics, Cambridge CB3 0WA, UK

<sup>5</sup>Kavli Institute for Cosmology Cambridge, Madingley Road, Cambridge CB3 0HA, UK

<sup>6</sup>H.H. Wills Physics Laboratory, Tyndall Avenue, Bristol BS8 1TL, UK

<sup>7</sup>Shanghai Astronomical Observatory, Shanghai, 200030, People’s Republic of China

<sup>8</sup>Niels Bohr International Academy, The Niels Bohr Institute, Blegdamsvej 17, DK-2100, Copenhagen, Denmark

Received 2025 May 20; revised 2025 November 9; accepted 2025 November 9; published 2025 November 25

## Abstract

It remains an open question whether the binary black hole (BBH) mergers observed with gravitational-wave detectors originate from the evolution of isolated massive binary stars or were dynamically driven by perturbations from the environment. Recent evidence for nonzero orbital eccentricity in a handful of events is seen as support for a nonnegligible fraction of the population experiencing external driving of the merger. However, it is unclear from *which* formation channel eccentric BBH mergers would originate: dense star clusters, hierarchical field triples, active galactic nuclei, or wide binaries in the galaxy could all be culprits. Here, we investigate whether the spin properties of eccentric mergers could be used to break this degeneracy. Using the fact that different formation channels are predicted to either produce eccentric mergers with mutually aligned or randomly oriented black hole spins, we investigate how many confident detections would be needed in order for the two models to be statistically distinguishable. If a few percent of BBH mergers retain measurable eccentricity in the bandwidth of ground-based detectors, we report a  $\sim 9\%$  chance that we could confidently distinguish both models (Bayes factor  $\ln \mathcal{B} > 3$ ) after the fifth observing run of the LIGO-Virgo-KAGRA detector network,  $\sim 63\%$  for LIGO A#, and  $\sim 98\%$  for the Einstein Telescope and Cosmic Explorer.

*Unified Astronomy Thesaurus concepts:* [Gravitational waves \(678\)](#); [Gravitational wave sources \(677\)](#); [Gravitational wave astronomy \(675\)](#); [Black holes \(162\)](#); [Eccentricity \(441\)](#); [Spin-orbit resonances \(2296\)](#); [Trinary stars \(1714\)](#); [Star clusters \(1567\)](#); [Wide binary stars \(1801\)](#); [Active galactic nuclei \(16\)](#)

## 1. Introduction

Ten years after the first direct detection of gravitational waves (GWs) from merging binary black holes (BBHs; B. P. Abbott et al. 2016), about 100 merger events have been observed (R. Abbott et al. 2023). However, the astrophysical mechanism forming them remains unclear. Multiple formation channels have been proposed, which can be broadly divided into two categories. On the one hand, isolated massive binary stars may develop merging BBHs after they have interacted through a stable mass-transfer episode (K. Inayoshi et al. 2017; E. P. J. van den Heuvel et al. 2017; S. S. Bavera et al. 2021; M. Gallegos-Garcia et al. 2021; P. Marchant et al. 2021; A. Olejak et al. 2021; J. Stegmann & F. Antonini 2021; L. A. C. van Son et al. 2022) in a common-envelope phase (K. A. Postnov & L. R. Yungelson 2014; K. Belczynski et al. 2016; J. J. Eldridge & J. R. Maund 2016; V. M. Lipunov et al. 2017; N. Giacobbo & M. Mapelli 2018) or in a chemically homogeneous evolution (S. E. de Mink & I. Mandel 2016; I. Mandel & S. E. de Mink 2016; L. du Buisson et al. 2020; J. Riley et al. 2021). On the other hand, BBHs may be driven to merge by some perturbation from the environment,

e.g., distant tertiary companions in hierarchical triples (O. Blaes et al. 2002; T. A. Thompson 2011; F. Antonini & H. B. Perets 2012; J. M. Antognini et al. 2014; F. Antonini et al. 2014; S. Prodan et al. 2015; K. Silsbee & S. Tremaine 2017; F. Antonini et al. 2018; ; E. Grishin et al. 2018; B.-M. Hoang et al. 2018; C. L. Rodriguez & F. Antonini 2018; J. Stegmann et al. 2022a, 2022b; A. Vigna-Gómez et al. 2025; J. Stegmann & J. Klencki 2025), scatterings in dense star clusters (J. Samsing et al. 2014; F. Antonini & F. A. Rasio 2016; C. L. Rodriguez et al. 2018; M. Zevin et al. 2021a; M. Mapelli et al. 2021; D. Chattopadhyay et al. 2023; M. Dall’Amico et al. 2024), flybys and the tidal field of the host galaxies (E. Michaely & H. B. Perets 2019; Y. Raveh et al. 2022; J. Stegmann et al. 2024), or gaseous embeddings in active galactic nuclei (AGNs; P. Goldreich et al. 2002; J. M. Bellovary et al. 2016; G. Fragione et al. 2019; H. Tagawa et al. 2020b; E. Grishin et al. 2024; M. P. Vaccaro et al. 2024; S. Gilbaum et al. 2025).

A powerful smoking-gun signature of the dynamical or otherwise externally perturbed formation of merging binaries is the presence of nonzero orbital eccentricity in a detected GW signal. This is because GW emission leads to extremely efficient angular momentum loss, which rapidly circularizes the orbit of a binary (P. C. Peters 1964). Thus, any system that retains a substantial residual eccentricity upon entering the sensitive frequency range of a ground-based GW detector must have formed with a much higher eccentricity. A fraction of



Original content from this work may be used under the terms of the [Creative Commons Attribution 4.0 licence](#). Any further distribution of this work must maintain attribution to the author(s) and the title of the work, journal citation and DOI.

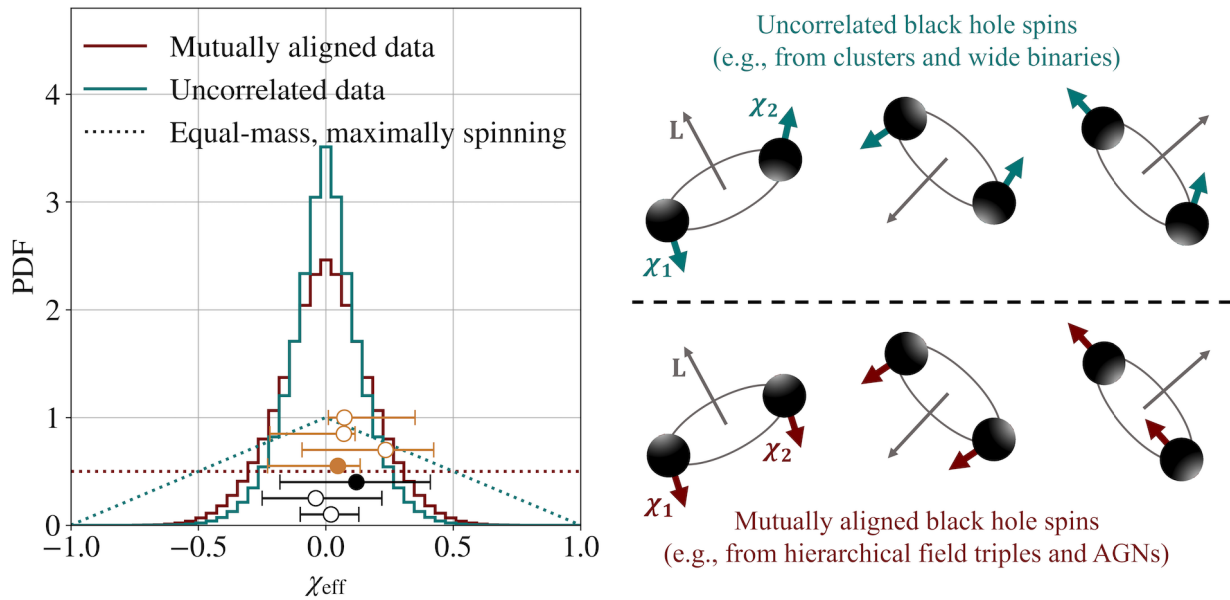


**Figure 1.** Left panel: distribution of  $\chi_{\text{eff}}$  for mutually aligned spin directions (maroon) and random spin directions (teal). Dotted lines indicate equal-mass ( $q = 1$ ) and maximally spinning BBHs ( $\chi_1 = \chi_2 = 1$ ), solid lines assume an extended mass ratio distribution and a spin magnitude distribution that peaks at lower values, which are consistent with previous GW detections (see Section 1). Black markers show three eccentric BBH merger candidates identified by N. Gupte et al. (2024; from bottom to top: GW200129, GW190701, and GW200208\_22), and orange markers show four candidates identified by I. Romero-Shaw et al. (2022; from bottom to top: GW200208\_22, GW190521, GW190620, and GW191109). The commonly identified candidate GW200208\_22 is highlighted by a filled marker (I. Romero-Shaw et al. 2025). Right panel: sketch of uncorrelated (top) and mutually aligned black hole spins of eccentric mergers (bottom).

BBH mergers with such large eccentricities is only expected if they are driven by an environmental perturbation. Conversely, the presence of nonzero eccentricity at the minimum sensitive frequency of ground-based detectors is wholly inconsistent with the expected evolution of isolated massive binary stars (e.g., K. Belczynski et al. 2002). Due to these considerations, the detection of even a few sources with nonzero eccentricity (or the lack thereof; M. Zevin et al. 2021a) would act as a “tip of the iceberg” and could be used to put constraints on the fraction of mergers formed from dynamical channels in the entire observed population (see V. Baibhav et al. 2020).

Tentative evidence for compact object mergers with nonzero eccentricity has recently been found in a handful of BBH merger events (e.g., I. Romero-Shaw et al. 2022; N. Gupte et al. 2024; H. L. Iglesias et al. 2024; M. de Lluc Planas et al. 2025), though degeneracies with misaligned spin are, at present, hard to eradicate (e.g., I. M. Romero-Shaw et al. 2023) (although, see e.g., K. Divyajyoti et al. 2024; G. Morras et al. 2025). If this evidence becomes more robust, it would suggest that a somewhat large fraction of the BBH mergers detected thus far formed through a dynamical formation channel. Here, we consider a scenario in which additional eccentric BBH merger events are confidently detected and investigate whether measuring their spin properties would further constrain which of the channels that produce eccentric mergers contribute. We focus on the spin properties because, for the subset of eccentric mergers, different formation channels make very distinct predictions. The two dimensionless spin vectors  $\chi_1$  and  $\chi_2$  of the black holes and their orbital angular momentum vector  $L$  are either expected to point in three random directions, or the spins are mutually closely aligned ( $\hat{\chi}_1 \approx \hat{\chi}_2$ ) but randomly oriented with respect to  $\hat{L}$ , as argued below and illustrated in the right panel of Figure 1.

- (i) Three random directions of  $\chi_1$ ,  $\chi_2$ , and  $L$  are a natural property of eccentric BBH mergers that form in dense

star clusters. There, BBHs that retain measurable eccentricity in the bandwidth of current GW detectors merge during resonant three- and four-body encounters that typically involve chaotic exchanges between binary members and scatterings that heavily perturb their orbits (J. Samsing et al. 2014; F. Antonini & F. A. Rasio 2016; C. L. Rodriguez et al. 2018; M. Zevin et al. 2021a; D. Chattopadhyay et al. 2023). In these chaotic encounters, merging BBHs are randomly assembled without any correlations between the spins and orbital angular momentum. As a result, the directions of  $\chi_1$ ,  $\chi_2$ , and  $L$  are independent of one another and effectively randomized.

- (ii) In contrast, closely aligned spins  $\hat{\chi}_1 \approx \hat{\chi}_2$  and a random direction of  $L$  are expected for eccentric BBH mergers that result from the evolution of hierarchical triples. In these systems, the BBHs are formed from massive binary stars whose spins are likely (closely) aligned to one another by stellar processes. The gravitational perturbation from a tertiary companion promotes a subsequent merger by causing large-amplitude von Zeipel–Kozai–Lidov (ZKL; H. V. Zeipel 1909; Y. Kozai 1962; M. L. Lidov 1962) oscillations of the BBH eccentricity and the orientation of its orbital angular momentum. BBHs that merge with a residual eccentricity undergo exceptionally strong ZKL oscillations, while the spin evolution is highly nonadiabatic, i.e., the orbital angular momentum vector oscillates several orders of magnitude quicker than the spins could follow it through relativistic spin–orbit coupling (F. Antonini et al. 2018; C. L. Rodriguez & F. Antonini 2018; B. Liu & D. Lai 2018; B. Liu et al. 2019). As a result, the eccentric BBH mergers retain the mutually aligned spins they inherited from their binary progenitor stars, while the direction of their orbital angular momentum vector is effectively randomized.

Other dynamical channels, such as BBHs merging due to the tidal field of the host galaxy and stellar flybys, as well as BBH mergers in AGNs, have been less studied in the context of spins in eccentric events. However, it is plausible to expect that they also fall into either one of the aforementioned categories.

First, BBHs that merge due to the perturbation from the galactic tidal field and flybys need to be exceptionally wide with semimajor axis  $\gtrsim 10^3$  au (J. Stegmann et al. 2024). Wide binaries are thought to form from initially unbound black holes that randomly pair up during the dissolution phase of young star clusters (M. B. N. Kouwenhoven et al. 2010), leading to uncorrelated directions of two spins and the orbital angular momentum vectors. Therefore, any eccentric BBH merger that originates from the evolution of wide massive binary stars would have three random directions of  $\chi_1$ ,  $\chi_2$ , and  $L$ .

In AGN disks, the spins of BBHs are expected to be mutually aligned through gas accretion due to the Bardeen–Petterson effect (J. M. Bardeen & J. A. Petterson 1975), in which the alignment of the black hole spin with a circum-black-hole disk proceeds much faster than the evolution of the spin magnitude (see B. McKernan et al. 2020; A. Santini et al. 2023 for related modeling). However, the directions of the orbital angular momentum can be misaligned with the black hole spin directions depending on the frequency of binary–single interactions. This frequency is influenced by the properties of the AGN disks, especially the merging locations within the AGN disks. Recent models predict frequent interactions with random angular momentum directions (H. Tagawa et al. 2020a). In these cases, the spin–orbit alignment for the AGN channel is predicted to be similar to that of the three-body channel, and highly eccentric mergers are expected for a fraction of mergers. On the other hand, for the AGN channel, hierarchical mergers are inevitable (Y. Yang et al. 2019; H. Tagawa et al. 2021; D. Gerosa & M. Fishbach 2021), resulting in high masses and spins for these black holes, which can help distinguish them from triple systems.

In this work, we study how many confident detections of eccentric BBH mergers we would need before the two spin–orbit configurations of (i) three randomly distributed directions of  $\chi_1$ ,  $\chi_2$ , and  $L$  and (ii) two randomly distributed directions of  $\chi_1$  and  $L$  and  $\hat{\chi}_1 \approx \hat{\chi}_2$  become statistically distinguishable. We highlight that focusing on spin–eccentricity correlations is particularly advantageous compared to previous approaches to distinguish formation channels from the marginalized spin distribution of all mergers (e.g., C. L. Rodriguez & F. Antonini 2018; C. L. Rodriguez et al. 2019; V. Baibhav & V. Kalogera 2024). First, eccentric mergers can *only* be explained by a reduced number of formation channels, as any residual eccentricity close to merger is inconsistent with isolated binary formation scenarios (G. Fumagalli et al. 2024). Instead, eccentric mergers *must* have formed through a formation channel involving dynamical driving. Second, models of such formation channels only predict the clear distinction in spin distributions (i) and (ii) for eccentric events. The majority of events that merge on effectively circular orbits can originate from a wider variety of channels and have a less certain spin distribution. For instance, a significant fraction of all mergers that form in triples is expected to have a spin–orbit precession timescale comparable or shorter than the ZKL timescale, which leads to a more diverse merger distribution of spin–orbit angles (B. Liu & D. Lai 2018;

C. L. Rodriguez & F. Antonini 2018). Meanwhile, an uncertain fraction of noneccentric mergers in clusters may originate from primordial stellar binaries that experience no or only few dynamical interactions (J. Barber et al. 2024) and whose spin directions do not fully randomize as in (i). Thus, while any viable formation channel must be consistent with the entire joint spin–eccentricity distribution, this work shows that its detectably eccentric subpopulation is particularly insightful to constrain merger origins.

## 2. Methods

We consider externally driven BBH mergers that retain some measurable eccentricity upon entering ground-based GW detectors, which we refer to as “eccentric BBHs.” It is typically assumed that orbital eccentricities above a threshold of several 0.01 at a nominal GW frequency of 10 Hz could be measurable for events detected by the LIGO–Virgo–KAGRA (LVK) detector network (M. E. Lower et al. 2018).

Dynamical formation channels that produce eccentric BBHs make distinct predictions about the relative directions of their orbital angular momentum vector  $L$  and the dimensionless spin vectors  $\chi_1$  and  $\chi_2$ . Whereas in some models (e.g., dense star clusters) eccentric BBHs are formed with  $L$ ,  $\chi_1$ , and  $\chi_2$  pointing in three independent random directions, in other models (e.g., hierarchical field triples), only  $L$  is randomized but  $\chi_1$  and  $\chi_2$  are (nearly) aligned. We stress that this is only true for the subset of eccentric mergers, whereas the entire population of mergers from a particular channel can follow more complicated distributions of the spins and the orbital angular momentum. These two predictions impact the effective spin parameter (T. Damour 2001):

$$\chi_{\text{eff}} = \frac{\chi_1 \cos \theta_1 + q \chi_2 \cos \theta_2}{1 + q}, \quad (1)$$

where  $0 < q \leq 1$  is the mass ratio between the two black holes,  $\chi_1$  ( $\chi_2$ ) is the spin magnitude of the heavier (lighter) black hole, and  $\cos \theta_1 = \hat{\chi}_1 \cdot \hat{L}$  and  $\cos \theta_2 = \hat{\chi}_2 \cdot \hat{L}$  are the cosines of the spin–orbit tilt angles. We focus on the effective spin parameter because it is usually the best-constrained spin parameter in GW measurements. Moreover, orbit-averaging the equations of motion of the BBHs,  $\chi_{\text{eff}}$  remains conserved during their inspiral (É. Racine 2008; D. Gerosa et al. 2023), i.e., its value is the same at BBH formation and merger. While the orbit-averaged approximation technically breaks down for highly eccentric mergers (G. Fumagalli et al. 2025), we demonstrate in Appendix A that resulting variations of  $\chi_{\text{eff}}$  are expected to be irrelevant for this work. A concise investigation of the evolution of the individual tilt angles  $\theta_{1,2}$  is presented in Appendix B.

Random directions of  $L$ ,  $\chi_1$ , and  $\chi_2$  correspond to uncorrelated distributions  $\cos \theta_1 \sim \mathcal{U}(-1, 1)$  and  $\cos \theta_2 \sim \mathcal{U}(-1, 1)$ . In contrast, random directions of  $L$  but mutually aligned spins mean  $\cos \theta_1 = \cos \theta_2 \sim \mathcal{U}(-1, 1)$ . We refer to these models as “uncorrelated” and “mutually aligned,” respectively. The difference between the distribution of  $\chi_{\text{eff}}$  in both models is maximized if we consider the unrealistic but instructive case of equal-mass ( $q = 1$ ) and maximally spinning ( $\chi_1 = \chi_2 = 1$ ) BBHs. This is shown in the left panel of Figure 1 (dotted lines), which illustrates that the mutually aligned model tends to produce more extreme values near  $\chi_{\text{eff}} \approx \pm 1$ , whereas the uncorrelated model is more

centered around zero. Both models resemble one another more closely if we consider more realistic, nonunity mass ratios and spin magnitudes. In Figure 1, this is shown with solid lines where we draw the mass ratio from a power-law distribution  $p(q) \sim q^\alpha$  between 0.1 and 1.0 and the spin magnitudes from some Beta distribution  $p(\chi_{1,2}) \sim \text{Beta}(a, b)$ . We choose fiducial values  $\alpha = 1.1$ ,  $a = 1.4$ , and  $b = 3.6$ , which are consistent with the distributions inferred from the GWTC-3 (R. Abbott et al. 2023). As a result, the mutually aligned model retains more pronounced tails of the distribution, whereas the uncorrelated model is more concentrated around  $\chi_{\text{eff}} = 0$ . Yet, the two distributions are more similar than in the previous case where  $q = \chi_1 = \chi_2 = 1$  due to a weaker contribution of the second term on the right-hand side of Equation (1).

Any attempt to statistically distinguish between both distributions with the current sample of eccentric candidate events (colored markers in Figure 1) would be preposterous, not only because of the small number statistics but also because they were identified using eccentric aligned spin waveform models, which may result in systematic biases against highly misaligned spins. However, we can estimate whether we could statistically prefer one model over the other with the growing data obtained from future GW observations and improved waveform modeling that accounts for precessing spins in eccentric events.

For this purpose, we assume a total number of  $N_{\text{tot}}$  detected BBH mergers, which we set to 2100 as a reference for the fifth observing run of LVK (LVK O5; F. S. Broekgaarden et al. 2024),  $10^4$  for A# (B. P. Abbott et al. 2020), and  $10^5$  for the Einstein Telescope (ET; A. Abac et al. 2025) and Cosmic Explorer (CE; D. Reitze et al. 2019). We assume that a fraction  $0 \leq \xi_{\text{ecc}} \leq 1$  of them will retain confidently measurable eccentricity in the detector sensitivity window, resulting in  $N_{\text{ecc}} = N_{\text{tot}} \times \xi_{\text{ecc}}$  eccentric BBHs (rounded to the next integer). We only consider events in  $N_{\text{ecc}}$  with sufficient evidence for eccentricity, i.e., assume a suitable selection function was applied that discards events with marginal evidence to avoid spurious contamination by circular events (I. Mandel et al. 2019; S. K. Roy et al. 2025). At present, constructing a suitable selection function that would only collect confident detections of eccentricity is difficult given that current eccentric waveform models disagree on eccentricity in most events (I. Romero-Shaw et al. 2022; N. Gupte et al. 2024). Here, we defer such a task to future work and rely on the number  $N_{\text{ecc}}$  of confident eccentric detections that could be obtained in that way. For each detector configuration, we repeat the following steps  $10^4$  times:

- (i) We produce a synthetic merger population by sampling  $N_{\text{ecc}}$  eccentric BBHs with mass ratios drawn from a power-law distribution  $p(q) \sim q^\alpha$  between 0.1 and 1.0 and spin magnitudes independently drawn from some Beta distribution  $p(\chi_{1,2}) \sim \text{Beta}(a, b)$ . We assume that the distribution parameters are drawn from  $\alpha \sim \mathcal{N}(1.1, 1.0)$ ,  $a \sim \mathcal{N}(1.4, 0.1)$ , and  $b \sim \mathcal{N}(3.6, 0.1)$ . The assumed uncertainty is based on the current spin magnitude distribution of GWTC-3 (R. Abbott et al. 2023), but we note it will likely improve in the future as more events are being detected. For each of the eccentric BBH mergers, we compute  $\chi_{\text{eff}}$  using Equation (1) assuming either mutually aligned or uncorrelated spin directions. Lastly, we approximate the posterior distribution of each  $\chi_{\text{eff}}$

measurement with a truncated normal distribution between  $-1$  and  $1$ , where the adopted standard deviation  $\sigma_{\chi_{\text{eff}}}$  represents typical measurement uncertainties.

- (ii) We construct mutually aligned and uncorrelated models that are tested against the synthetic GW data constructed in step (i). To this end, we repeat step (i)  $N \gg N_{\text{ecc}}$  times with a different set of parameters drawn from  $\alpha \sim \mathcal{N}(1.1, 1.0)$ ,  $a \sim \mathcal{N}(1.4, 0.1)$ , and  $b \sim \mathcal{N}(3.6, 0.1)$ . These values are considered as a proxy for the best-fit values that can be obtained from the distribution of all mergers  $N_{\text{tot}}$ .
- (iii) Having constructed a synthetic population of eccentric mergers in step (i) and uncorrelated and mutually aligned models based on spin magnitude and mass ratio samples obtained from all detected mergers in step (ii), we compute Bayes factor

$$\mathcal{B} = \frac{p(\text{Data}|\text{Model})}{p(\text{Data}|\text{Alternative Model})}, \quad (2)$$

where

$$p(\text{Data}|\text{Model}) = \prod_{i=1}^{N_{\text{ecc}}} p_{\text{Model}}(|\chi_{\text{eff},i}|). \quad (3)$$

Here,  $p_{\text{Model}}$  is a linear interpolation of the normalized distribution of  $|\chi_{\text{eff}}|$  obtained in step (ii), and  $\chi_{\text{eff},i}$  are the effective spin parameter values of the eccentric BBH mergers synthesized in step (i). In Equation (3), we consider distributions of the absolute value of  $\chi_{\text{eff}}$  because our models for  $\chi_{\text{eff}}$  are symmetric around zero (see Figure 1).

Repeating steps (i) to (iii), we obtain Bayes factor distributions for

$$\mathcal{B} = \frac{p(\text{Mutually aligned data}|\text{Mutually aligned model})}{p(\text{Mutually aligned data}|\text{Uncorrelated data})} \quad (4)$$

and

$$\mathcal{B} = \frac{p(\text{Uncorrelated data}|\text{Uncorrelated model})}{p(\text{Uncorrelated data}|\text{Mutually aligned model})} \quad (5)$$

to quantify the confidence to recover the correct model, i.e., the mutually aligned model in the presence of mutually aligned data and the uncorrelated model in the presence of uncorrelated data. In the discussion below, we follow R. E. Kass & A. E. Raftery (1995) and consider  $2 \ln \mathcal{B} \gtrsim 6$  (i.e.,  $\log_{10} \mathcal{B} \gtrsim 1.3$ ) to indicate strong evidence for the correct model,  $-6 \lesssim 2 \ln \mathcal{B} \lesssim 6$  ( $-1.3 \lesssim \log_{10} \mathcal{B} \lesssim 1.3$ ) to indicate no particular preference for either model, and  $2 \ln \mathcal{B} \lesssim -6$  ( $\log_{10} \mathcal{B} \lesssim -1.3$ ) to indicate strong evidence for the incorrect model.

If not stated otherwise, we assume an eccentric merger fraction of  $\xi_{\text{ecc}} = 0.05$ , which agrees with predictions from dynamical channels for current ground-based detectors (e.g., F. Antonini et al. 2014; M. Zevin et al. 2021a) and is consistent with the order of magnitude of eccentric candidates in the current population of GW events (I. Romero-Shaw et al. 2022; N. Gupte et al. 2024). However, it likely underestimates the fraction of eccentric mergers detectable with the next-generation detectors ET/CE, as they will be sensitive to smaller eccentricities (A. Dorozsmay et al. 2025, in

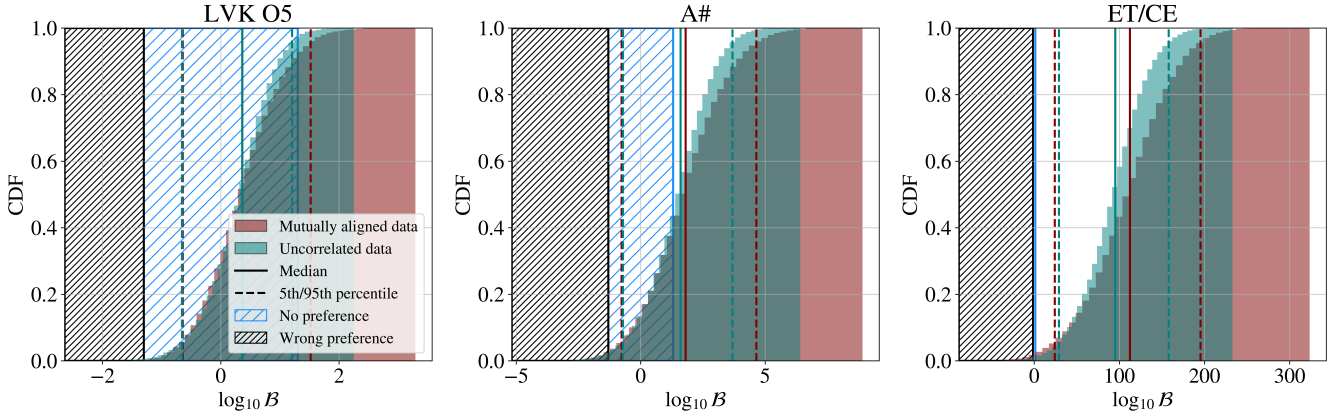


**Figure 2.** Bayes factor distributions that compare the mutually aligned and uncorrelated models. The maroon histogram assumes GW detections of systems with mutually aligned spins and indicates the confidence for preferring the aligned model over the uncorrelated model. Conversely, the teal histogram assumes GW detections of systems with uncorrelated spins and indicates the confidence for preferring the uncorrelated spin model over the mutually aligned spin model. Thus, in either case, a large Bayes factor ( $\log_{10} \mathcal{B} \gtrsim 1.3$ ) indicates that we would correctly infer the spin properties of the underlying population. Solid and dashed vertical lines indicate the medians and 5th/95th percentiles of the distributions, respectively. We assume an eccentric BBH fraction of  $\xi_{\text{ecc}} = 0.05$ , a measurement uncertainty for  $\chi_{\text{eff}}$  of  $\sigma_{\chi_{\text{eff}}} = 0.2$  for LVK O5 and A# and  $\sigma_{\chi_{\text{eff}}} = 0.02$  for ET/CE, and vary between each panel the total number of detections between 2, 100 (LVK O5),  $10^4$  (A#), and  $10^5$  (ET/CE).

preparation). Below, we also study different values for  $\xi_{\text{ecc}}$ . For the measurement uncertainty of  $\chi_{\text{eff}}$ , we assume as a default  $\sigma_{\chi_{\text{eff}}} = 0.2$  for LVK O5 and A#, which is the typical uncertainty of the (quasi-circular) events identified in GWTC-3. We assume that ET/CE will allow measurements that are more precise by 1 order of magnitude,  $\sigma_{\chi_{\text{eff}}} = 0.02$ . Since it is unclear at what precision next-generation detectors will measure  $\chi_{\text{eff}}$  of eccentric events, we also study different values  $\sigma_{\chi_{\text{eff}}}$ .

We note that step (i) implicitly assumes that eccentric and noneccentric mergers share the same distribution of black hole spin magnitudes, modeled as a Beta distribution. This assumption is justified because black hole spin magnitudes are primarily determined by the physics of stellar core collapse, which is largely independent of the environment in which the binary forms. Different spin magnitudes may only arise from hierarchical mergers in dense stellar clusters, which can produce highly spinning black holes with  $\chi_i \simeq 0.7$  (D. Gerosa & M. Fishbach 2021). However, the contribution of such “second-generation” mergers to the eccentric subset as well as all mergers is expected to be small (e.g., C. L. Rodriguez et al. 2019; M. Mapelli et al. 2021).

It could also be possible that multiple formation channels contribute to the total merger rate. This would only significantly impact our analysis if these channels contributed comparably and had substantially different spin magnitude distributions. Such a scenario would require a degree of fine-tuning. In contrast, the eccentric merger fraction  $\xi_{\text{ecc}}$  considered in this work is consistent with all mergers being dominated by dynamical formation processes. In these channels, only a subset of binaries retains measurable eccentricity within the sensitivity range of our detectors, while the rest is formed through the same mechanism but circularized before entering the detectable eccentricity regime. Moreover, any alternative formation channel would need to produce a markedly different spin distribution, which is unlikely given that spin magnitudes are predominantly governed by core-collapse physics.

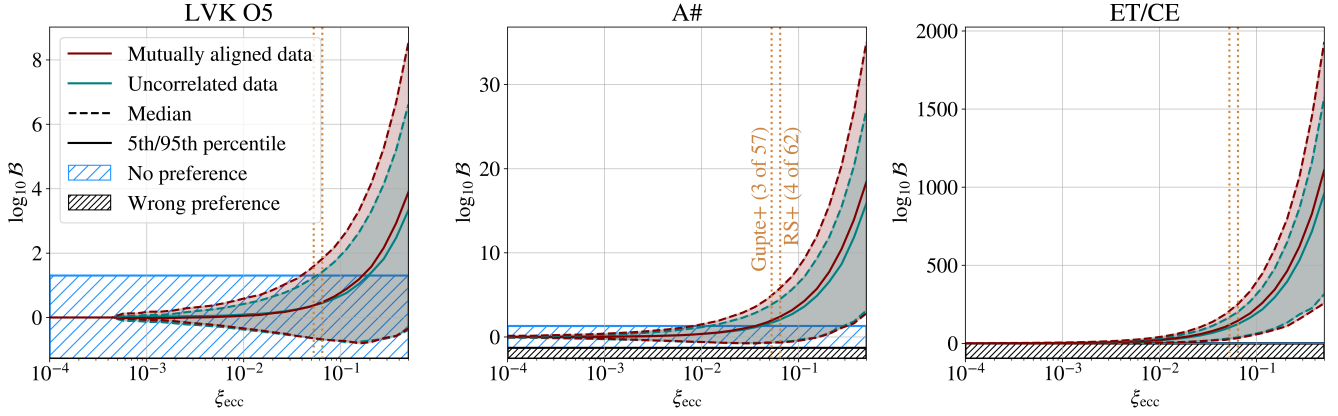
### 3. Results

Figure 2 shows the Bayes factor distributions for the three detector configurations LVK O5 (right panel), A# (middle

panel), and ET/CE (right panel) for our default assumptions  $\xi_{\text{ecc}} = 0.05$  and  $\sigma_{\chi_{\text{eff}}} = 0.2$  for LVK O5 and A# and  $\sigma_{\chi_{\text{eff}}} = 0.02$  for ET/CE. If the eccentric BBH mergers form with mutually aligned spins (“mutually aligned data”, maroon histograms), the Bayes factors for statistically preferring the mutually aligned spin model over the uncorrelated spin model range from  $\log_{10} \mathcal{B} = 0.37_{-0.99}^{+1.14}$  (LVK O5) and  $\log_{10} \mathcal{B} = 1.84_{-2.55}^{+2.77}$  (A#) to  $\log_{10} \mathcal{B} = 111_{-84}^{+87}$  (ET/CE), where uncertainties refer to the 5th/95th percentiles. Similarly, for eccentric BBH mergers with uncorrelated spins (“Uncorrelated data”, teal histograms), we find Bayes factors for recovering the uncorrelated spin model over the mutually aligned spin model ranging from  $\log_{10} \mathcal{B} = 0.36_{-0.97}^{+0.83}$  (LVK O5) and  $\log_{10} \mathcal{B} = 1.61_{-2.27}^{+2.05}$  (A#) to  $\log_{10} \mathcal{B} = 95_{-62}^{+66}$  (ET/CE). We consider  $\log_{10} \mathcal{B} \gtrsim 1.3$  (nonhatched region) as a minimal threshold for substantial evidence to prefer the correct model. This is the case for  $\sim 9\%$  of the realizations in LVK O5,  $\sim 63\%$  for A#, and  $\sim 98\%$  for ET/CE. Meanwhile, obtaining substantial evidence for preferring the incorrect model ( $\log_{10} \mathcal{B} \lesssim -1.3$ ) happens for  $\sim 1\%$  of the realizations in all detectors. Thus, in all detector configurations, the probability of preferring the incorrect model is low. However, only with A# and ET/CE do we expect a large probability to infer the correct model at high significance and thus to be able to statistically distinguish the dynamical origin of the eccentric BBHs. For LVK O5, it is most likely that the data will show no strong preference for either model.

For our default assumptions ( $\xi_{\text{ecc}} = 0.05$  and  $\sigma_{\chi_{\text{eff}}} = 0.2$  for LVK O5 and A# and  $\sigma_{\chi_{\text{eff}}} = 0.02$  for ET/CE), we also checked the expected statistics for the ongoing fourth observing run of LVK. Assuming a total number of  $N_{\text{tot}} = 500$  detections, we find  $\log_{10} \mathcal{B} = 0.07_{-0.43}^{+0.56}$  and  $\log_{10} \mathcal{B} = 0.10_{-0.49}^{+0.37}$  for mutually aligned and uncorrelated data, respectively. We conclude that it is very unlikely that these models can be distinguished with O4 data.

In Figure 3, we vary the eccentric merger fraction  $\xi_{\text{ecc}}$  (while keeping our default measurement uncertainty of  $\sigma_{\chi_{\text{eff}}} = 0.2$  for LVK O5 and A# and  $\sigma_{\chi_{\text{eff}}} = 0.02$  for ET/CE). For LVK O5, A#, and ET/CE, we find a minimum eccentric merger fraction of  $\xi_{\text{ecc}} \gtrsim 21\%$ ,  $5\%$ , and  $0.08\%$ ,



**Figure 3.** Percentiles of the Bayes factor distributions as a function of the eccentric BBH fraction  $\xi_{\text{ecc}}$ . We assume that  $\chi_{\text{eff}}$  will be measured with an uncertainty of  $\sigma_{\chi_{\text{eff}}} = 0.2$  for LVK O5 and A# and  $\sigma_{\chi_{\text{eff}}} = 0.02$  for ET/CE. As in Figure 2, solid and dashed lines indicate the median and 5th/95th percentiles, respectively. The vertical yellow dotted lines indicate the eccentric fraction of events identified by N. Gupte et al. (2024; 3 of 57 analyzed events; “Gupte+”) and by I. Romero-Shaw et al. (2022; 4 of 62 analyzed events; “RS+”), respectively.

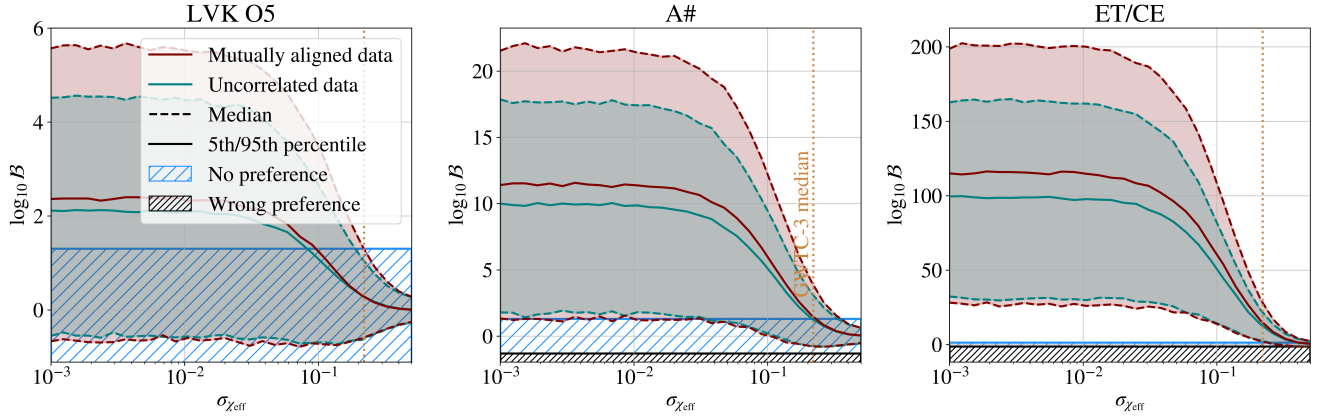


**Figure 4.** Percentiles of the Bayes factor distributions as a function of the eccentric BBH fraction and the measurement uncertainty  $\sigma_{\chi_{\text{eff}}}$  of  $\chi_{\text{eff}}$ . We assume an eccentric BBH fraction of  $\xi_{\text{ecc}} = 0.05$ . The vertical yellow dotted line indicates the typical uncertainty obtained in GWTC-3.

respectively, is needed so that the median of the Bayes factor distributions exceeds  $\log_{10} \mathcal{B} \approx 1.3$ . The 5th percentile would exceed  $\log_{10} \mathcal{B} \approx 1.3$  if  $\xi_{\text{ecc}} \gtrsim 37\%$  (A#) and  $0.6\%$  (ET/CE), respectively, whereas the 5th percentile remains below  $\log_{10} \mathcal{B} \approx 1.3$  for LVK O5.

In Figure 4, we vary the measurement uncertainty  $\sigma_{\chi_{\text{eff}}}$  (while keeping our default eccentric merger fraction  $\xi_{\text{ecc}} = 0.05$ ). For LVK O5, A#, and ET/CE, we find that it must not be greater than  $\sigma_{\chi_{\text{eff}}} \approx 0.09, 0.21,$  and  $0.40$ , respectively, for the median to exceed  $\log_{10} \mathcal{B} \approx 1.3$ . The 5th percentile would have  $\log_{10} \mathcal{B} \approx 1.3$  if  $\sigma_{\chi_{\text{eff}}} \lesssim 0.03$  (A#) and  $0.21$  (ET/CE), respectively. Thus, we also repeated our entire analysis by conservatively assuming that the measurement uncertainty  $\sigma_{\chi_{\text{eff}}}$  of eccentric sources with ET/CE does not improve but will be the same as for LVK O5 and A#, i.e.,  $\sigma_{\chi_{\text{eff}}} = 0.2$  (instead of our default assumption of  $0.02$ ). We find that this only marginally affects our conclusions, demonstrating that it is primarily the large number of detections with ET/CE that will allow distinguishing between both models. In particular, we find that still  $\sim 96\%$  of the realizations with  $\xi_{\text{ecc}} = 0.05$  will have  $\log_{10} \mathcal{B} \gtrsim 1.3$  (compared to the  $\sim 98\%$  for  $\sigma_{\chi_{\text{eff}}} = 0.02$ ) and  $\sim 0.02\%$  have  $\log_{10} \mathcal{B} \lesssim 1.3$  (instead of  $\sim 0.01\%$ ).

Above, we assumed that in the mutually aligned model, the two spins are perfectly aligned to one another, i.e.,  $\hat{\chi}_1 = \hat{\chi}_2$ .

Generally, mutually aligned spins can be the result of massive binary stars whose stellar spins synchronize due to tides or other stellar binary interactions and whose black hole remnants inherit the alignment before driven to an eccentric merger due to the environment (e.g., tertiary companions in hierarchical triples or AGNs). However, some misalignment might occur if, e.g., the stars are born with uncorrelated spins or misalign during a mass-transfer episode (J. Stegmann & F. Antonini 2021) but tides are too inefficient to align them; the black holes form with spins that do not inherit the orientation from the rotation axes of the progenitor stars (V. Baibhav & V. Kalogera 2024); or supernova kicks tilt the direction of the orbital angular momentum (V. Kalogera 2000; D. Gerosa et al. 2018; N. Steinle & M. Kesden 2021). Thus, we investigate another “tilted model,” where, instead of setting  $\hat{\chi}_1 = \hat{\chi}_2$ , we sample  $\hat{\chi}_1 \cdot \hat{\chi}_2$  uniformly between 1 and a given minimum value  $\min(\hat{\chi}_1 \cdot \hat{\chi}_2) \in [-1, 1)$  and assume a random azimuthal angle of  $\hat{\chi}_2$  about  $\hat{\chi}_1$ . In Figure 5, we assume that the eccentric BBH mergers form with tilted spins (“tilted data”) with some minimum value  $\min(\hat{\chi}_1 \cdot \hat{\chi}_2)$  shown on the  $x$ -axis (with our default assumptions  $\xi_{\text{ecc}} = 0.05$  and  $\sigma_{\chi_{\text{eff}}} = 0.2$  for LVK O5 and A# and  $\sigma_{\chi_{\text{eff}}} = 0.02$  for ET/CE). Maroon and teal percentiles of  $\log_{10} \mathcal{B}$  show how well we could recover the tilted model over the aligned and uncorrelated models, respectively. Note that for  $\min(\hat{\chi}_1 \cdot \hat{\chi}_2) = -1$  and  $+1$ , the tilted

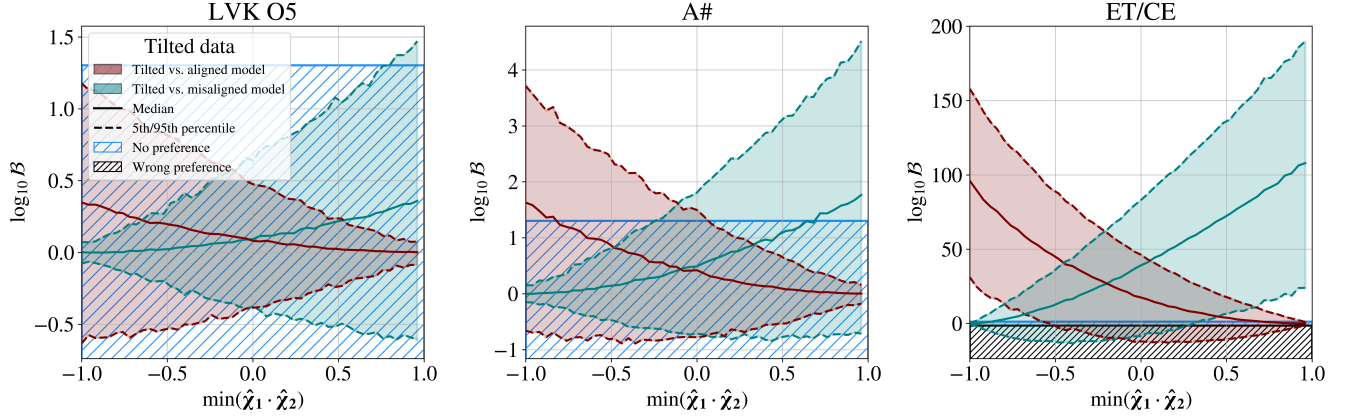


**Figure 5.** Percentiles of the Bayes factor distributions that compare the uncorrelated model (teal) to a tilted model (maroon), where we allow the spins to be tilted with respect to one another by  $\min(\hat{\chi}_1 \cdot \hat{\chi}_2)$ . We assume an eccentric BBH fraction of  $\xi_{\text{ecc}} = 0.05$  and a measurement uncertainty for  $\chi_{\text{eff}}$  of  $\sigma_{\chi_{\text{eff}}} = 0.2$  for LVK O5 and A# and  $\sigma_{\chi_{\text{eff}}} = 0.02$  for ET/CE.

model is equivalent to the uncorrelated and mutually aligned model, respectively. Thus, the test against the mutually aligned model (maroon) converges to  $\log_{10} \mathcal{B} = 0$  as  $\min(\hat{\chi}_1 \cdot \hat{\chi}_2) \rightarrow 1$ , and the test against the uncorrelated model (teal) goes to zero as  $\min(\hat{\chi}_1 \cdot \hat{\chi}_2) \rightarrow -1$ . Crucially, the tilted model will be statistically preferred against the uncorrelated model (teal) even if we allow large spin–spin misalignments, e.g., the teal median is  $\log_{10} \mathcal{B} \gtrsim 1.3$  for  $\min(\hat{\chi}_1 \cdot \hat{\chi}_2) \gtrsim 0.7$  for A# and for  $\gtrsim -0.9$  for ET/CE, respectively. Astrophysically, that means that we would be able to distinguish formation channels in which the spin direction would fully randomize, e.g., clusters, from those that tend to align the spins, e.g., hierarchical triples, even if we allow significant tilt angles between them.

#### 4. Conclusion

Identifying the formation channel of BBH mergers is a major quest in GW astronomy. While eccentricity is a smoking-gun signature of dynamical assembly or the influence of a tertiary, several channels that produce eccentric mergers may contribute to the observed merger rate. In this work, we show that spin measurements, when restricted to the subpopulation of eccentric mergers, can delineate *which* of these channels is at play.

Specifically, we investigated if  $\chi_{\text{eff}}$  measurements of eccentric BBH mergers can be used to distinguish between models with mutually aligned and randomly oriented spins, which would help to identify the dynamical formation channel through which they must have formed. For our default assumptions, corresponding to an eccentric merger fraction  $\xi_{\text{ecc}} = 0.05$  and measurement uncertainty  $\sigma_{\chi_{\text{eff}}} = 0.2$  for LVK O5 and A# and  $\sigma_{\chi_{\text{eff}}} = 0.02$  for ET/CE, we find an  $\sim 9\%$  chance to confidently distinguish both models after LVK O5,  $\sim 63\%$  for LIGO A#, and  $\sim 98\%$  for ET and CE (Figure 2). These results depend significantly on  $\xi_{\text{ecc}}$  and the future values of  $\sigma_{\text{eff}}$ , both of which are uncertain, and may correlate. Parameter estimation studies using eccentric waveform models have shown correlations between  $\chi_{\text{eff}}$  and eccentricity, which could cause wider uncertainties on  $\chi_{\text{eff}}$  if detected eccentricity is poorly constrained (E. O’Shea & P. Kumar 2023; K. Divyajyoti et al. 2024); however, we note that since future ground-based GW detectors will be able to constrain

eccentricities about 2 orders of magnitude lower than current detectors (P. Saini 2024), this effect is likely to be small.

Finally, we note that our analysis is simplistic in four ways. First, we have not included any noneccentric detections to distinguish between formation channels of BBH mergers. Since current models predict  $\xi_{\text{ecc}} \lesssim \mathcal{O}(0.1)$ , a given number of eccentric mergers necessarily implies there is a much larger number of circularized mergers originating from the same channel. Thus, any viable formation channel must not only recover the spin–orbit properties of eccentric mergers but also be consistent with the rest of the population, where multiple channels (including isolated binary star evolution) might contribute (M. Zevin et al. 2021b). In turn, focusing on the eccentric mergers has the advantage that we know they must originate from a dynamical or triple channel and that these channels make distinct predictions for the spin–orbit properties. Second, we did not consider the possibility that multiple channels contribute to the formation of eccentric mergers. We expect this to influence our analysis only if they contribute at about the same order of magnitude, in which case in step (ii) of Section 2, a mixture model must be constructed that contains a fraction  $0 < \beta < 1$  of mutually aligned mergers and a fraction  $1 - \beta$  of uncorrelated ones. Third, we approximated the posterior distribution of  $\chi_{\text{eff}}$  with a truncated normal distribution, but note that in reality, asymmetries may arise (e.g., K. K. Y. Ng et al. 2018). However, we do not expect this to significantly change our qualitative results. Furthermore, establishing robust correlations between measurable eccentricity and binary spin remains an open problem in the field. Our analysis is strictly valid in the high-signal-to-noise ratio (SNR) regime; should selection effects due to eccentricity–spin measurements prove to be significant, the methodology presented in this Letter can be straightforwardly applied to a higher-purity subset of the catalog, obtained by imposing a more stringent SNR threshold. While this would increase the required number of detections, it would not alter the qualitative conclusions of the approach.

#### Acknowledgments

We thank the Sexten Center for Astrophysics, where this work was kickstarted. We thank Johan Samsing, Ilya Mandel, Fabio Antonini, and the anonymous referee for useful input and discussions. J.S. acknowledges funding from NWO Vidi

grant No. 639.042.728–BinWaves. D.G. and G.F. are supported by ERC Starting grant No. 945155–GWmining, Cariplo Foundation grant No. 2021-0555, MUR PRIN grant No. 2022-Z9X4XS, MUR grant “Progetto Dipartimenti di Eccellenza 2023-2027” (BiCoQ), and the ICSC National Research Centre funded by NextGenerationEU. D.G. is supported by MSCA Fellowship No. 101064542–StochRewind, MSCA Fellowship No. 101149270–ProtoBH, and MUR Young Researchers grant No. SOE2024-0000125. I.M.R.-S. acknowledges the support of the Herchel Smith fund.

## Appendix A

### Evolution of $\chi_{\text{eff}}$ during Eccentric BBH Inspirals

During the inspiral of a BBH, the effective spin parameter  $\chi_{\text{eff}}$  is a conserved quantity at second post-Newtonian (PN) order when averaging over orbital motion (É. Racine 2008; D. Gerosa et al. 2023). On highly eccentric orbits, the orbit-averaged approximation may break down if efficient GW emission at close periapsis passages induces changes of the orbital elements on a timescale smaller than the orbital period. As a result, the black hole spins may precess about the orbital angular momentum vector without conserving  $\chi_{\text{eff}}$  so that our method to use  $\chi_{\text{eff}}$  at BBH formation as a proxy for  $\chi_{\text{eff}}$  at BBH merger would break down. In order to estimate our error, we simulate the inspiral of 1000 BBHs using the publicly available regularized direct  $N$ -body integrator MSTAR (A. Rantala et al. 2020; M. Mannerkoski et al. 2023), which uses the Gragg–Bulirsch–Stoer extrapolation technique (W. B. Gragg 1965; R. Bulirsch & J. Stoer 1966) to account for the mutual gravitational interaction between the  $N=2$  black holes to 3.5PN order (T. Mora & C. M. Will 2004). The integration is terminated if the BBHs get as close as 12 combined Schwarzschild radii. The BBHs are initialized on a highly eccentric orbit

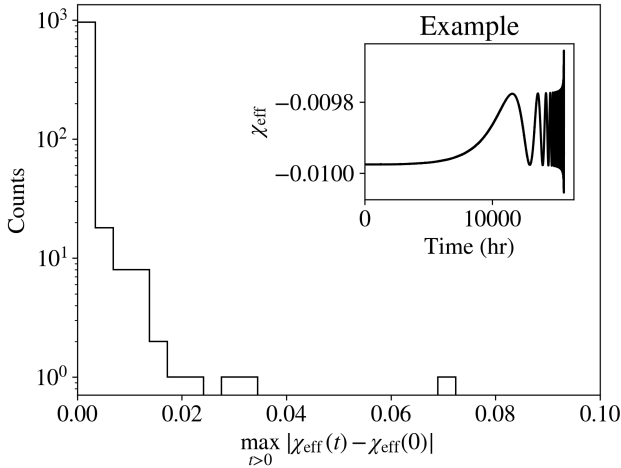


**Figure 6.** Distribution of the maximum difference  $\max_{t>0} |\chi_{\text{eff}}(t) - \chi_{\text{eff}}(0)|$  of  $\chi_{\text{eff}}$  during the inspirals of our BBH sample with initially aligned spins and high eccentricity. The inset exemplifies the time evolution of  $\chi_{\text{eff}}$  of a typical system.

with eccentricity  $e = 0.999$ , total mass  $m = 30 M_{\odot}$ , and periapsis  $r_p = 300M$ , where  $M = Gm/c^2$ . The mass ratio of the BBHs is drawn from a power-law distribution  $p(q) \sim q^{\alpha}$  between 0.1 and 1.0 and the spin magnitudes from some Beta distribution  $p(\chi_{1,2}) \sim \text{Beta}(a, b)$  with our fiducial parameters  $\alpha = 1.1$ ,  $a = 1.4$ , and  $b = 3.6$ . The BBHs are initialized at apoapsis, and their spins are assumed to be aligned. Figure 6 shows that for the majority of BBH inspirals,  $\chi_{\text{eff}}$  does not oscillate by more than  $\sim 0.02$  and none of them by more than  $\sim 0.1$  around the initial values. Based on these simulations, we conclude that our results are not significantly affected by treating  $\chi_{\text{eff}}$  as a conserved quantity.

## Appendix B

### Evolution of $\cos \theta_1$ and $\cos \theta_2$ during Eccentric BBH Inspirals

Unlike the effective spin parameter  $\chi_{\text{eff}}$ , the spin tilt angles do not remain constant during the inspiral. Instead, they precess within precession cones whose amplitudes evolve due to GW emission while remaining effectively fixed on the shorter precession timescale. The presence of distinct timescales in the dynamics allows for an efficient treatment of spin evolution through a double-averaging procedure: first over the orbital timescale and then over the precession timescale (D. Gerosa et al. 2015, 2023). This technique has been successfully applied to study spin-precession, quasi-circular BBHs and, more recently, eccentric systems as well (G. Fumagalli & D. Gerosa 2023). Using the extended version of the precession code presented by G. Fumagalli & D. Gerosa (2023), we investigate the evolution of the spin tilts in a population of eccentric BBHs in the mutually aligned and uncorrelated models as described in Section 1. We simulate  $10^5$  binaries with total mass  $M = 20M_{\odot}$ . The mass ratios are drawn from a power-law distribution  $p(q) \sim q^{\alpha}$  with  $\alpha = 1.1$  and  $q \in [0.1, 1.0]$ ; spin magnitudes are either sampled from a Beta distribution  $p(\chi_{1,2}) \sim \text{Beta}(a, b)$  with  $a = 1.4$  and  $b = 3.6$  or fixed to the maximal value  $\chi_1 = \chi_2 = 1$ . BBHs are assumed to form with the initial eccentricity  $e = 0.999$  and semimajor axis  $a \sim 1.1 \times 10^5 GM/c^2$ , corresponding to a GW frequency  $f_{\text{GW}} \sim 0.95$  Hz. We evolve the systems until they reach an eccentricity of  $e = 0.1$  at  $f_{\text{GW}} = 10$  Hz.

Figure 7 shows the resulting evolution of the spin tilts  $\theta_{1,2}$ . As previously reported in quasi-circular binaries (T. Bogdanović et al. 2007; D. Gerosa et al. 2015), initially isotropic (i.e., uncorrelated) spin tilt distributions remain isotropic throughout the inspiral, even in the presence of eccentricity (G. Fumagalli & D. Gerosa 2023). On the other hand, deviations appear in the case of initially aligned spin tilts. In these systems, the spin tilt distributions evolve away from mutual alignment, exhibiting a tendency to cluster around  $\cos \theta_i = \pm 1$ . This behavior, already identified in the quasi-circular case (D. Gerosa et al. 2013), is here found to persist in the eccentric regime as well. The effect is especially pronounced in the maximally spinning case, consistent with the expectation that spin–orbit and spin–spin couplings are stronger for higher spin magnitudes.

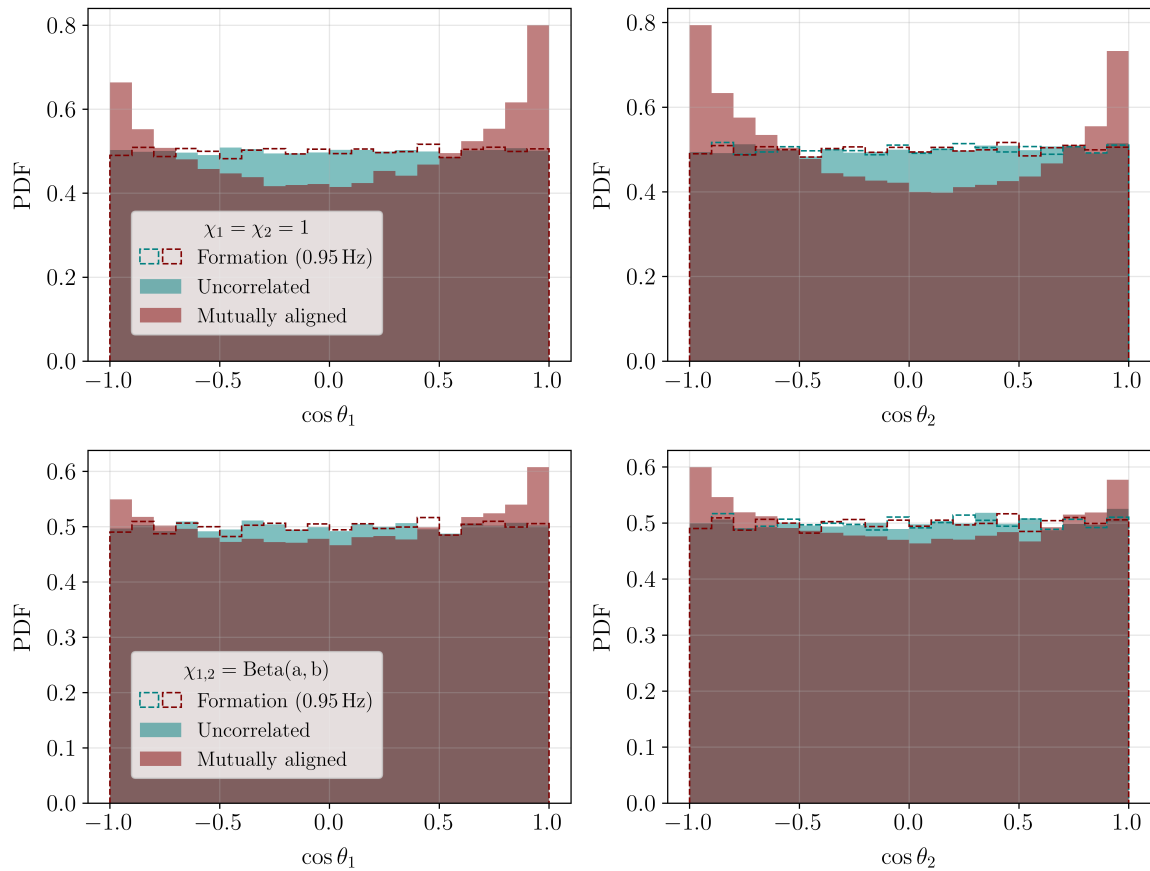


**Figure 7.** Distribution of the cosine of spin tilt angles,  $\cos \theta_1$  (left panels) and  $\cos \theta_2$  (right panels). We assume spin tilts to be either mutually aligned (maroon) or uncorrelated (teal) at formation. Distributions at detection ( $f_{\text{GW}} = 10$  Hz) and BBH formation ( $f_{\text{GW}} = 0.95$  Hz) are shown as a filled and dashed histogram, respectively. We assume either maximally spinning BH (top panels) or spin magnitudes extracted from a Beta distribution as in Figure 2 (bottom panels).

### ORCID iDs

Jakob Stegmann <https://orcid.org/0000-0003-2340-8140>  
 Davide Gerosa <https://orcid.org/0000-0002-0933-3579>  
 Isobel Romero-Shaw <https://orcid.org/0000-0002-4181-8090>  
 Giulia Fumagalli <https://orcid.org/0009-0004-2044-989X>  
 Hiromichi Tagawa <https://orcid.org/0000-0002-5674-0644>

### References

- Abac, A., Abramo, R., Albanesi, S., et al. 2025, arXiv:2503.12263  
 Abbott, B. P., Abbott, R., Abbott, T. D., et al. 2016, *PhRvL*, **116**, 061102  
 Abbott, B. P., Abbott, R., Abbott, T. D., et al. 2020, *LRR*, **23**, 3  
 Abbott, R., Abbott, T. D., Acernese, F., et al. 2023, *PhRvX*, **13**, 011048  
 Antonini, J. M., Shappee, B. J., Thompson, T. A., & Amaro-Seoane, P. 2014, *MNRAS*, **439**, 1079  
 Antonini, F., Murray, N., & Mikkola, S. 2014, *ApJ*, **781**, 45  
 Antonini, F., & Perets, H. B. 2012, *ApJ*, **757**, 27  
 Antonini, F., & Rasio, F. A. 2016, *ApJ*, **831**, 187  
 Antonini, F., Rodriguez, C. L., Petrovich, C., & Fischer, C. L. 2018, *MNRAS*, **480**, L58  
 Baibhav, V., Gerosa, D., Berti, E., et al. 2020, *PhRvD*, **102**, 043002  
 Baibhav, V., & Kalogera, V. 2024, arXiv:2412.03461  
 Barber, J., Chattopadhyay, D., & Antonini, F. 2024, *MNRAS*, **527**, 7363  
 Bardeen, J. M., & Petterson, J. A. 1975, *ApJL*, **195**, L65  
 Bavera, S. S., Fragos, T., Zevin, M., et al. 2021, *A&A*, **647**, A153  
 Belczynski, K., Kalogera, V., & Bulik, T. 2002, *ApJ*, **572**, 407  
 Belczynski, K., Repetto, S., Holz, D. E., et al. 2016, *ApJ*, **819**, 108  
 Bellovary, J. M., Mac Low, M.-M., McKernan, B., & Ford, K. E. S. 2016, *ApJL*, **819**, L17  
 Blaes, O., Lee, M. H., & Socrates, A. 2002, *ApJ*, **578**, 775  
 Bogdanović, T., Reynolds, C. S., & Miller, M. C. 2007, *ApJL*, **661**, L147  
 Broekgaarden, F. S., Banagiri, S., & Payne, E. 2024, *ApJ*, **969**, 108  
 Bulirsch, R., & Stoer, J. 1966, *NuMat*, **8**, 1  
 Chattopadhyay, D., Stegmann, J., Antonini, F., Barber, J., & Romero-Shaw, I. M. 2023, *MNRAS*, **526**, 4908  
 Dall’Amico, M., Mapelli, M., Torniamenti, S., & Arca Sedda, M. 2024, *A&A*, **683**, A186  
 Damour, T. 2001, *PhRvD*, **64**, 124013  
 de Lluc Planas, M., Ramos-Buades, A., García-Quirós, C., et al. 2025, arXiv:2504.15833  
 de Mink, S. E., & Mandel, I. 2016, *MNRAS*, **460**, 3545  
 Divyjayoti, K., Tibrewal, S., Romero-Shaw, I. M., & Mishra, C. K. 2024, *PhRvD*, **109**, 043037  
 du Buisson, L., Marchant, P., Podsiadlowski, P., et al. 2020, *MNRAS*, **499**, 5941  
 Eldridge, J. J., & Maund, J. R. 2016, *MNRAS*, **461**, L117  
 Fragione, G., Grishin, E., Leigh, N. W. C., Perets, H. B., & Perna, R. 2019, *MNRAS*, **488**, 47  
 Fumagalli, G., & Gerosa, D. 2023, *PhRvD*, **108**, 124055  
 Fumagalli, G., Loutrel, N., Gerosa, D., & Boschini, M. 2025, *PhRvD*, **112**, 024012  
 Fumagalli, G., Romero-Shaw, I., Gerosa, D., et al. 2024, *PhRvD*, **110**, 063012  
 Gallegos-Garcia, M., Berry, C. P. L., Marchant, P., & Kalogera, V. 2021, *ApJ*, **922**, 110  
 Gerosa, D., Berti, E., O’Shaughnessy, R., et al. 2018, *PhRvD*, **98**, 084036  
 Gerosa, D., & Fishbach, M. 2021, *NatAs*, **5**, 749  
 Gerosa, D., Fumagalli, G., Mould, M., et al. 2023, *PhRvD*, **108**, 024042  
 Gerosa, D., Kesden, M., Berti, E., O’Shaughnessy, R., & Sperhake, U. 2013, *PhRvD*, **87**, 104028  
 Gerosa, D., Kesden, M., Sperhake, U., Berti, E., & O’Shaughnessy, R. 2015, *PhRvD*, **92**, 064016  
 Giacobbo, N., & Mapelli, M. 2018, *MNRAS*, **480**, 2011  
 Gilbaum, S., Grishin, E., Stone, N. C., & Mandel, I. 2025, *ApJL*, **982**, L13  
 Goldreich, P., Lithwick, Y., & Sari, R. 2002, *Natur*, **420**, 643  
 Gragg, W. B. 1965, *SJNA*, **2**, 384  
 Grishin, E., Gilbaum, S., & Stone, N. C. 2024, *MNRAS*, **530**, 2114

- Grishin, E., Perets, H. B., & Fragione, G. 2018, *MNRAS*, 481, 4907
- Gupte, N., Ramos-Buades, A., Buonanno, A., et al. 2024, arXiv:2404.14286
- Hoang, B.-M., Naoz, S., Kocsis, B., Rasio, F. A., & Dosopoulou, F. 2018, *ApJ*, 856, 140
- Iglesias, H. L., Lange, J., Bartos, I., et al. 2024, *ApJ*, 972, 65
- Inayoshi, K., Hirai, R., Kinugawa, T., & Hotokezaka, K. 2017, *MNRAS*, 468, 5020
- Kalogera, V. 2000, *ApJ*, 541, 319
- Kass, R. E., & Raftery, A. E. 1995, *JASA*, 90, 773
- Kouwenhoven, M. B. N., Goodwin, S. P., Parker, R. J., et al. 2010, *MNRAS*, 404, 1835
- Kozai, Y. 1962, *AJ*, 67, 591
- Lidov, M. L. 1962, *P&SS*, 9, 719
- Lipunov, V. M., Kornilov, V., Gorbvskoy, E., et al. 2017, *NewA*, 51, 122
- Liu, B., & Lai, D. 2018, *ApJ*, 863, 68
- Liu, B., Lai, D., & Wang, Y.-H. 2019, *ApJ*, 881, 41
- Lower, M. E., Thrane, E., Lasky, P. D., & Smith, R. 2018, *PhRvD*, 98, 083028
- Mandel, I., & de Mink, S. E. 2016, *MNRAS*, 458, 2634
- Mandel, I., Farr, W. M., & Gair, J. R. 2019, *MNRAS*, 486, 1086
- Mannerkoski, M., Rawlings, A., Johansson, P. H., et al. 2023, *MNRAS*, 524, 4062
- Mapelli, M., Dall'Amico, M., Bouffanais, Y., et al. 2021, *MNRAS*, 505, 339
- Marchant, P., Pappas, K. M. W., Gallegos-Garcia, M., et al. 2021, *A&A*, 650, A107
- McKernan, B., Ford, K. E. S., O'Shaugnessy, R., & Wysocki, D. 2020, *MNRAS*, 494, 1203
- Michaely, E., & Perets, H. B. 2019, *ApJL*, 887, L36
- Mora, T., & Will, C. M. 2004, *PhRvD*, 69, 104021
- Morras, G., Pratten, G., & Schmidt, P. 2025, arXiv:2503.15393
- Ng, K. K. Y., Vitale, S., Zimmerman, A., et al. 2018, *PhRvD*, 98, 083007
- Olejak, A., Belczynski, K., & Ivanova, N. 2021, *A&A*, 651, A100
- O'Shea, E., & Kumar, P. 2023, *PhRvD*, 108, 104018
- Peters, P. C. 1964, *PhRv.*, 136, 1224
- Postnov, K. A., & Yungelson, L. R. 2014, *LRR*, 17, 3
- Prodan, S., Antonini, F., & Perets, H. B. 2015, *ApJ*, 799, 118
- Racine, É. 2008, *PhRvD*, 78, 044021
- Rantala, A., Pihajoki, P., Mannerkoski, M., Johansson, P. H., & Naab, T. 2020, *MNRAS*, 492, 4131
- Raveh, Y., Michaely, E., & Perets, H. B. 2022, *MNRAS*, 514, 4246
- Reitze, D., Adhikari, R., Ballmer, S., et al. 2019, *BAAS*, 51, 35
- Riley, J., Mandel, I., Marchant, P., et al. 2021, *MNRAS*, 505, 663
- Rodriguez, C. L., Amaro-Seoane, P., Chatterjee, S., et al. 2018, *PhRvD*, 98, 123005
- Rodriguez, C. L., & Antonini, F. 2018, *ApJ*, 863, 7
- Rodriguez, C. L., Zevin, M., Amaro-Seoane, P., et al. 2019, *PhRvD*, 100, 043027
- Romero-Shaw, I., Lasky, P. D., & Thrane, E. 2022, *ApJ*, 940, 171
- Romero-Shaw, I., Stegmann, J., Tagawa, H., et al. 2025, *PhRvD*, 112, 063052
- Romero-Shaw, I. M., Gerosa, D., & Loutrel, N. 2023, *MNRAS*, 519, 5352
- Roy, S. K., van Son, L. A. C., & Farr, W. M. 2025, arXiv:2507.01086
- Saini, P. 2024, *MNRAS*, 528, 833
- Samsing, J., MacLeod, M., & Ramirez-Ruiz, E. 2014, *ApJ*, 784, 71
- Santini, A., Gerosa, D., Cotesta, R., & Berti, E. 2023, *PhRvD*, 108, 083033
- Silsbee, K., & Tremaine, S. 2017, *ApJ*, 836, 39
- Stegmann, J., & Antonini, F. 2021, *PhRvD*, 103, 063007
- Stegmann, J., Antonini, F., & Moe, M. 2022a, *MNRAS*, 516, 1406
- Stegmann, J., Antonini, F., Schneider, F. R. N., Tiwari, V., & Chattopadhyay, D. 2022b, *PhRvD*, 106, 023014
- Stegmann, J., & Klencki, J. 2025, *ApJL*, 991, L54
- Stegmann, J., Vigna-Gómez, A., Rantala, A., et al. 2024, *ApJL*, 972, L19
- Steinle, N., & Kesden, M. 2021, *PhRvD*, 103, 063032
- Tagawa, H., Haiman, Z., Bartos, I., & Kocsis, B. 2020a, *ApJ*, 899, 26
- Tagawa, H., Haiman, Z., & Kocsis, B. 2020b, *ApJ*, 898, 25
- Tagawa, H., Kocsis, B., Haiman, Z., et al. 2021, *ApJ*, 908, 194
- Thompson, T. A. 2011, *ApJ*, 741, 82
- Vaccaro, M. P., Mapelli, M., Périgois, C., et al. 2024, *A&A*, 685, A51
- van den Heuvel, E. P. J., Portegies Zwart, S. F., & de Mink, S. E. 2017, *MNRAS*, 471, 4256
- van Son, L. A. C., de Mink, S. E., Renzo, M., et al. 2022, *ApJ*, 940, 184
- Vigna-Gómez, A., Grishin, E., Stegmann, J., et al. 2025, *A&A*, 699, A272
- Yang, Y., Bartos, I., Haiman, Z., et al. 2019, *ApJ*, 876, 122
- Zeipel, H. V. 1909, *AN*, 183, 345
- Zevin, M., Bavera, S. S., Berry, C. P. L., et al. 2021b, *ApJ*, 910, 152
- Zevin, M., Romero-Shaw, I. M., Kremer, K., Thrane, E., & Lasky, P. D. 2021a, *ApJL*, 921, L43